The electronic structures, Born effective charge tensors, and phonon properties of cubic, tetragonal, orthorhombic, and rhombohedral $K_{0.5}Na_{0.5}NbO_3$: A first-principles comparative study*

Zhou Shu-Lan(周树兰)[a)†], Zhao Xian(赵 显)[b)], Jiang Xiang-Ping(江向平)[a)], and Han Xiao-Dong(韩晓东)[a)]

[a)] *Department of Material Science and Engineering, Jingdezhen Ceramics Institute, Jingdezhen* 333403, *China*
[b)] *State Key Laboratory of Crystal Material, Institute of Crystal Material, Shandong University, Jinan* 250100, *China*

(Received 13 March 2014; revised manuscript received 1 August 2014; published online 10 October 2014)

The electronic structures, Born effective charges (BECs), and full phonon dispersions of cubic, tetragonal, orthorhombic, and rhombohedral $K_{0.5}Na_{0.5}NbO_3$ are investigated by the first principles method based on density functional theory. The hybridized states of Nb 4d and O 2p states are observed in the valence band, showing the formation of a strong Nb–O covalent bond which should be responsible for the displacement of Nb and O atoms. The abnormally large BECs of Nb and O indicate the possibility of phase instability induced by the off-center displacement of Nb and O atoms. The phonon dispersions reveal that the ferroelectric instability of $K_{0.5}Na_{0.5}NbO_3$ is dominated by Nb and O displacements with significant Na characteristics. In addition to the ferroelectric instability, there is also rotational instability coming from the oxygen octahedra rotation around one axis. Moreover, the Γ phonon properties of orthorhombic $KNbO_3$, $NaNbO_3$, and $K_{0.5}Na_{0.5}NbO_3$ are also studied in detail.

Keywords: Born effective charge, phonon dispersion, density functional theory (DFT), phase instability of $K_{0.5}Na_{0.5}NbO_3$

PACS: 71.20.–b, 77.84.–s, 62.60.+v **DOI:** 10.1088/1674-1056/23/12/127102

1. Introduction

Sodium potassium niobate is one of the most promising candidates of lead-free piezoelectric materials because of its relatively low dielectric permittivity, high electro-mechanical coupling coefficient, and high Curie temperature.[1–4] $K_{0.5}Na_{0.5}NbO_3$ (KNN), a combination of ferroelectrics $KNbO_3$ (KN) and anti-ferroelectrics $NaNbO_3$ (NN), has been reported to possess good piezoelectric properties (as it is near the morphotropic phase boundary), a moderate dielectric constant (ranging from 300 to 600), and a relatively large piezoelectric coefficient (d_{33} ~80 pC/N–120 pC/N).[5] Considerable efforts have been made to improve the piezoelectric property of KNN.[6–12] For example, by an ordinary sintering technique, Lin *et al*. prepared the CuO-doped KNN lead-free ceramics which possesses an extraordinarily high mechanical quality factor Q_m (825–2523). $BiFeO_3$-doped KNN exhibits enhanced ferroelectric, piezoelectric, and electro-mechanical properties of remanent polarization $P_r = 23.3$ μC/cm^2, $d_{33} = 185$ pC/N, and electromechanical planar coupling coefficient $k_p = 46\%$.[10] Zhou *et al*. fabricated dense ceramics of Ta-doped KNN, which exhibited optimum piezoelectric properties of $d_{33} = 210$ pC/N and good electromechanical coupling factors of $k_p = 0.3$.[11]

Efforts have also been devoted to the growth of a KNN crystal[7,13–15] and the phase transition process.[16–20] The studies show that KNN undergoes the same series of phases (cubic–tetragonal–orthorhombic–rhombohedral) (C–T–O–R) with a falling temperature, which is common to many perovskite ferroelectrics, in particular, to KN.[16,19,20] Lin *et al*. have grown the KNN crystal by using a high temperature flux method and investigated the ferroelectric phase transition temperatures, including the rhombohedral–orthorhombic, orthorhombic–tetragonal, and tetragonal–cubic transition temperatures.[13] However, the mechanism of the phase instability of KNN has not been investigated in depth. The electronic structure,[21–23] Born effective charge (BEC),[23–25] and phonon properties[23,24,26,27] play an important role in understanding the origin of ferroelectricity and the phase instability. Therefore, in order to investigate the micromechanism of phase instability of KNN, in this work, the electronic structures, BECs, and full phonon dispersions of cubic (KNNC), tetragonal (KNNT), orthorhombic (KNNO), and rhombohedral (KNNR) KNN are calculated by the first principles method based on the density functional theory. In addition, the Γ phonon properties of orthorhombic KN (KNO) and NN (NNO) are also calculated to investigate the role of K and Na anions in the ferroelectric instability of KNNO.

*Project supported by the Jiangxi Provincial Natural Science Foundation, China (Grant No. 20122BAB216007) and the Foundation of Jiangxi Provincial Educational Committee, China (Grant No. GJJ14648).

†Corresponding author. E-mail: zhoushulan2009@126.com

© 2014 Chinese Physical Society and IOP Publishing Ltd

2. Computational details

In order to simulate the properties of KNNC, KNNT, KNNO, and KNNR, the supercell with a 1:1 ratio of K to Na are shown in Fig. 1. Therefore, calculated structures of the several phases of KNN have the $P4/mmm$, $P4mm$, $Pmm2$, and $R3$ symmetries.

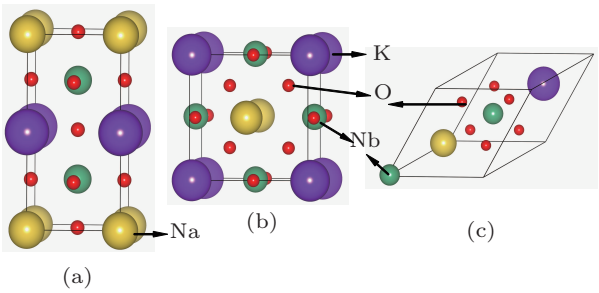


Fig. 1. (color online) Structures of KNNs: (a) KNNC and KNNT, (b) KNNO, and (c) KNNR.

The electronic structure calculations are performed by the plane-wave pseudopotential method based on density functional theory[28] as implemented in CASTEP.[29] The exchange–correlation effects were treated within the local density approximation. The interactions between ionic cores and valence electrons were represented by the norm conserving pseudopotentials[30] with $2s^22p^4$, $2s^22p^63s^1$, $3s^23p^64s^1$, and $4s^24p^64d^45s^1$ serving as the valence electron configurations for the oxygen, sodium, potassium, and niobium, respectively. Geometry optimizations were achieved using convergence thresholds of 5.0×10^{-6} eV/atom for total energy, 5.0×10^{-4} Å for displacement, 0.01 eV/Å for maximum force, and 0.02 Gpa for pressure. The BECs and phonon properties were calculated using density-functional perturbation theory as implemented in ABINIT.[31] For all the calculations, the plane-wave basis set energy cut-off was set at 50 Hatree (1 Hartree = 27.2114 eV). The Monkhorst–Pack scheme k-point grid samplings were set at $6\times6\times3$, $6\times6\times3$, $6\times4\times4$, and $4\times4\times4$ for KNNC, KNNT, KNNO, and KNNR, respectively. For cubic KN, KNO, and NNO, the $6\times6\times6$ k-point grid sampling was used in the calculations.

3. Results and discussion

3.1. Crystal structure

The calculated structure parameters of KNNC, KNNT, KNNO, and KNNR are presented in Table 1. Observing the internal coordinates of KNNT, KNNO, and KNNR, it is found that K, Na, Nb, and O are displaced along the pseudocubic [001], [011], and [111] direction relative to those of KNNC. Hence, the displacements of the atoms along the polar axis would make the structure stable.

Table 1. Calculated structure parameters for KNNC, KNNT, KNNO, and KNNR

Structure	Atom	Site	x	y	z	Å
KNNC	Na	1a	0.0000	0.0000	0.0000	$a=b=3.9689$
	K	1b	0.0000	0.0000	0.5000	$c=7.9339$
	Nb	2h	0.5000	0.5000	0.2477	
	O1	4i	0.0000	0.5000	0.2448	
	O2	1c	0.5000	0.5000	0.0000	
	O3	1d	0.5000	0.5000	0.5000	
KNNT	Na	1a	0.0000	0.0000	0.0284	$a=b=3.9466$
	K	1a	0.0000	0.0000	0.5108	$c=8.0881$
	Nb	1b	0.5000	0.5000	0.2637	
	Nb	1b	0.5000	0.5000	0.7702	
	O1	2c	0.5000	0.0000	0.2385	
	O2	2c	0.5000	0.0000	0.7482	
	O3	1b	0.5000	0.5000	-0.0010	
	O4	1b	0.5000	0.5000	0.4945	
KNNO	K	1a	0.0000	0.0000	0.0130	$a=3.9348$
	Na	1b	0.0000	0.5000	0.4744	$b=5.6449$
	Nb1	1c	0.5000	0.0000	0.5003	$c=5.6817$
	Nb2	1d	0.5000	0.5000	0.9971	
	O1	1a	0.0000	0.0000	0.5336	
	O2	1b	0.0000	0.5000	0.0436	
	O3	2h	0.5000	0.2531	0.2831	
	O4	2h	0.5000	0.7496	0.7790	
KNNR	Na	1a	0.2718	0.2718	0.2718	$a=b=c=5.6334$
	K	1a	0.7571	0.7571	0.7571	$\alpha=\beta=\gamma=59.6547^\circ$
	Nb	1a	0.0119	0.0119	0.0119	
	Nb	1a	0.5125	0.5125	0.5125	
	O1	3b	0.7427	0.2332	0.2661	
	O2	3b	0.2480	0.7853	0.7138	

3.2. Electronic structure

Figure 2 shows the calculated band structures of KNNC, KNNT, KNNO, and KNNR along high-symmetric directions in the Brillouin zone. It is observed that the tops of the valence band and the bottoms of the conduction band of KNNC, KNNT, and KNNO are located at different symmetric points, indicating the indirect-band gap nature of the three structures. While for KNNR, those are located at the same symmetry point, showing a direct band gap. The calculated gaps are 1.371 eV, 1.280 eV, 1.799 eV, and 2.201 eV for KNNC, KNNT, KNNO, and KNNR, respectively. The band structure of KNNT shows similar features to that of KNNC with a minor difference; the band structures of KNNO and KNNR seem to be different from those of KNNC and KNNT, owing to the use of different supercells. To facilitate the comparison of the electronic structures, the total densities of states (TDOSs) and partial densities of states (PDOSs) of the four structures are calculated and displayed in Fig. 3.

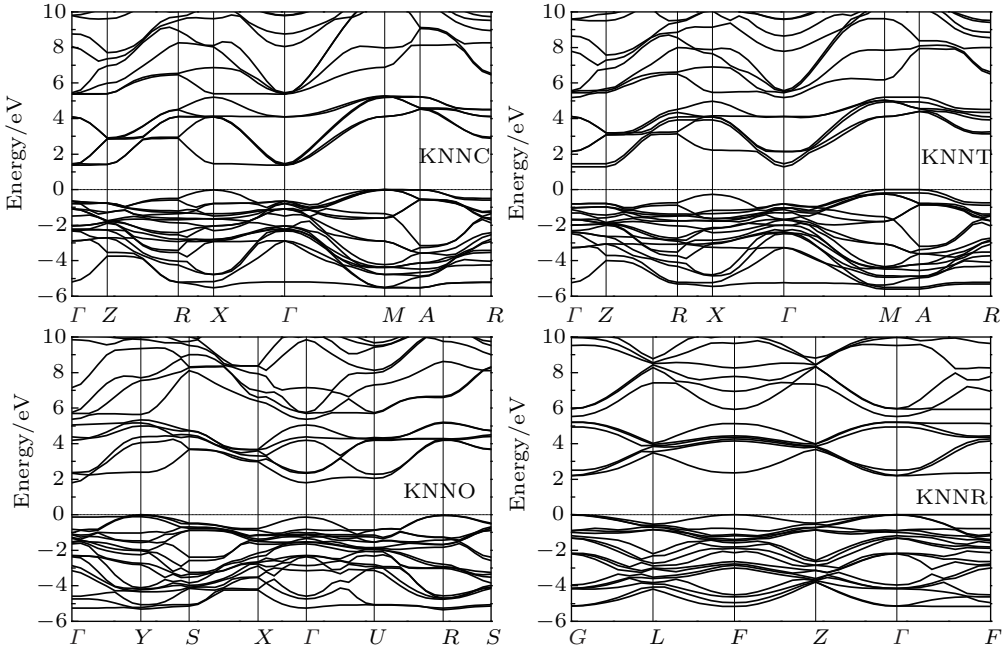


Fig. 2. Band structures of KNNC, KNNT, KNNO, and KNNR.

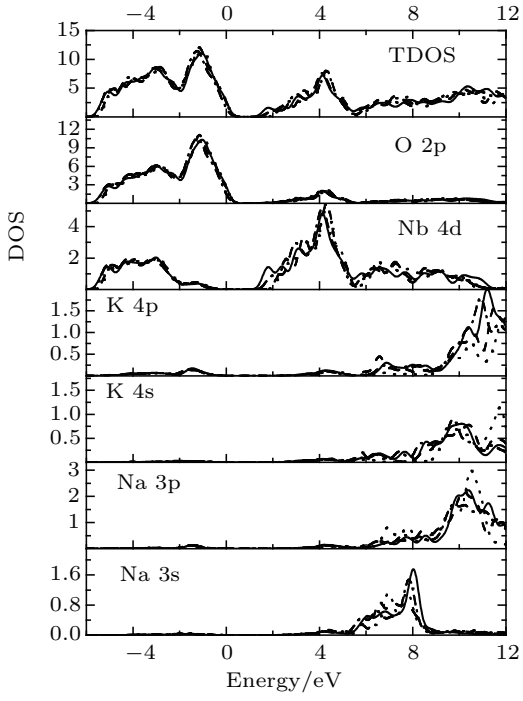


Fig. 3. TDOSs and PDOSs of KNNC (solid line), KNNT (dash–dotted line), KNNO (dashed line), and KNNR (dotted line).

As shown in Fig. 3, the TDOSs of KNNC, KNNT, KNNO, and KNNR are very similar. Oxygen p-states make primary contributions to the valence bands of all the four studied structures. The additional valence band contains contributions mostly from Nb 4d states. In the valence band (from −5.5 eV to 0 eV), the admixture of O 2p and Nb 4d electron states is significant, showing the formation of a strong covalent bond. The lower conduction bands (from 1.5 eV to 5.5 eV) are dominated by Nb 4d states, while the upper conduction bands (above 6 eV) consist of Nb 4d, K 4s4p, and Na 3s3p states. However, differences can also be clearly observed in the PDOSs of Nb 4d, Na 3s3p, and K 4s4p. For KNNT, KNNO, and KNNR, the bottoms of the conduction band shift toward a higher energy region relative to that of KNNC. The position and strength of the peaks vary in a range from 2 eV to 5 eV depending on the structures. The peaks of Na 3s3p and K 4s4p in the conduction band also vary obviously in different phases. In addition, minor differences can be found between different phases in the O 2p and Nb 4d valence bands. The evolutions of DOS in the four structures probably indicate the variations of the interactions of Nb–O, K–O, and Na–O bonds.

3.3. BEC tensor

As is well known, an anomalously large BEC Z^* of an atom is a general feature of a perovskite compound such as titanate, zirconate, and niobate,[24] which is associated with its excellent ferroelectric and piezoelectric properties. Table 2 gives the calculated Born effective charge tensors of KNNC, KNNT, KNNO, and KNNR. Owing to higher local site symmetries of Na, K, Nb, and O for KNNC and KNNT, and of O1 and O2 for KNNO, their respective effective charge tensors are diagonal. On the other hand, the BEC tensors of O3 and O4 for KNNO and of all atoms for KNNR are neither isotropic nor diagonal due to lower local site symmetry. For all the four structures, the effective charges of Nb and O atoms deviate significantly from their nominal ionic values, indicating the mixed ionic covalent Nb–O bonding due to the hybridization of O 2p orbitals with Nb 4d orbitals mentioned above, while the values of effective charges for the K and Na ions are quite close to their nominal ionic value of +1. This indicates that the Na–O and K–O bonding essentially remain ionic.

The effective charge tensor of O atoms has three independent components which are parallel to the x (Z^*_{xx}), y (Z^*_{yy}), and z (Z^*_{zz}) axes, respectively. As shown in Table 2, for KNNC, the calculated values of −7.57, −7.67, and −7.51 are three times higher than the nominal ionic value of −2. The charge tensor components (9.93 and 9.95) of Nb atoms are also anomalously large. As is well known, the large BEC of ions is related to the large displacement associated with ferroelectric instability.[32] Consequently, the displacements of the Nb and O atoms along the x, y, and z axes are probably responsible for the ferroelectric phase transition. For KNNT, the effective charges show features similar to those for KNNC. However, the charge tensor components along the z axis decrease to 7.02 and 7.12 for Nb and −5.30 and −5.63 for O, respectively. This reveals that the Nb–O bond along z axis becomes more covalent, indicating that the structure of KNNT is stable relative to that of KNNC along this axis. Compared with the components of KNNC, the components of KNNO along the y and z axes both decrease (to 8.25, 8.24, 7.37, and 7.26 for Nb; to −3.94, −4.01, −3.45, and −3.47 for O), showing stronger covalent interaction between Nb–O along these directions. Therefore, KNNO structures shows a further phase stability relative to those of KNNC and KNNT.

Table 2. BEC tensors of KNNC, KNNT, KNNO, and KNNR.

Structure	Atom	Site	Z^*_{xx}	Z^*_{xy}	Z^*_{xz}	Z^*_{yx}	Z^*_{yy}	Z^*_{yz}	Z^*_{zx}	Z^*_{zy}	Z^*_{zz}
KNNC	Na	1*a*	1.11	0.00	–0.00	0.00	1.11	–0.00	0.00	0.00	1.11
	K	1*b*	1.02	0.00	–0.00	–0.00	1.02	–0.00	–0.00	0.00	1.02
	Nb	2*h*	9.93	0.00	0.00	0.00	9.93	0.00	0.00	0.00	9.95
	O1	4*i*	–7.57	0.00	–0.00	–0.00	–1.71	0.00	0.00	0.00	–1.71
	O2	1*c*	–1.71	0.00	–0.00	–0.00	–1.71	0.00	–0.00	0.00	–7.67
	O3	1*d*	–1.71	0.00	–0.00	0.00	–1.71	0.00	0.00	0.00	–7.51
KNNT	Na	1*a*	1.11	0.00	0.00	0.00	1.11	0.00	0.00	0.00	1.15
	K	1*a*	1.04	0.00	0.00	0.00	1.04	0.00	0.00	0.00	1.08
	Nb1	1*b*	9.47	0.00	0.00	0.00	9.47	0.00	0.00	0.00	7.02
	Nb2	1*b*	9.29	0.00	0.00	0.00	9.29	0.00	0.00	0.00	7.12
	O1	2c	–7.38	0.00	0.00	0.00	–1.70	0.00	0.00	0.00	–1.36
	O2	2c	–7.17	0.00	0.00	0.00	–1.73	0.00	0.00	0.00	–1.37
	O3	1*b*	–1.48	0.00	0.00	0.00	–1.48	0.00	0.00	0.00	–5.30
	O4	1*b*	–1.46	0.00	0.00	0.00	–1.46	0.00	0.00	0.00	–5.63
KNNO	Na	1*a*	1.12	0.00	0.00	0.00	1.19	0.00	0.00	0.00	1.13
	K	1*b*	1.04	0.00	0.00	0.00	1.06	0.00	0.00	0.00	1.04
	Nb1	1*c*	9.43	0.00	0.00	0.00	8.26	0.00	0.00	0.00	7.37
	Nb2	1*d*	9.05	0.00	0.00	0.00	8.25	0.00	0.00	0.00	7.26
	O1	1*a*	–7.33	0.00	0.00	0.00	–1.40	0.00	0.00	0.00	–1.49
	O2	1*b*	–7.08	0.00	0.00	0.00	–1.45	0.00	0.00	0.00	–1.46
	O3	2*h*	–1.61	0.00	0.00	0.00	–3.94	–2.20	0.00	–2.34	–3.45
	O4	2*h*	–1.50	0.00	0.00	0.00	–4.01	–2.30	0.00	–2.46	–3.47
KNNR	Na	1*a*	1.12	–0.01	–0.04	–0.04	1.15	0.03	0.01	–0.05	1.15
	K	1*a*	1.03	–0.01	0.01	0.00	1.04	–0.02	–0.02	0.02	1.04
	Nb1	1*a*	7.72	–0.66	–0.12	–0.33	8.30	–0.60	–0.58	0.20	8.45
	Nb2	1*a*	7.85	–0.17	–0.46	–0.49	8.24	0.26	–0.01	–0.53	8.33
	O1	3*b*	–1.46	0.16	0.12	0.26	–4.69	–2.31	0.22	–2.33	–3.13
			–3.73	1.62	–1.92	1.49	–2.51	1.26	–1.88	1.30	–3.05
			–3.68	–1.30	2.12	–1.30	–2.23	1.28	2.01	1.18	–3.38
	O2	3*b*	–1.47	0.16	0.08	0.27	–4.77	–2.28	0.14	–2.24	–2.95
			–3.63	1.49	–1.93	1.40	–2.42	1.27	–1.92	1.36	–3.13
			–3.74	–1.28	2.15	–1.25	–2.11	1.12	2.03	1.08	–3.33

However, the charges of Nb and O along the x and y axes for KNNT and along the x axis for KNNO are still large, indicating that the instabilities along these directions are caused by the displacements of Nb and O atoms. For KNNR, all the values of the effective charges of Nb and O are smaller than for KNNC, therefore the structure is most stable. This will be consistent with the analysis of phonon dispersion in Subsection 3.4.

3.4. Phonon properties

The full phonon-dispersion relations can give information about the lattice instabilities and local distortions in ferroelectric oxides. The calculated phonon dispersion curves of KNNC, KNNT, KNNO, and KNNR along high-symmetry directions are shown in Fig. 4. Imaginary phonon frequencies (of unstable modes) are represented as negative values. We will pay attention mainly to the unstable ('soft') modes, for they are relevant to the phase transitions. For comparison, the phonon dispersions of cubic KN are calculated and displayed in Fig. 5. It is noted that our calculated results are in good agreement with those given by Yu and Krakauer,[33] showing the reliability of our calculations.

The instability of the structure of KNNC is clearly observed from the phonon dispersion (see Fig. 4). The most unstable mode is at Γ and dominated by the Nb displacement against the oxygen atoms along [100] direction with significant characteristic of Na displacement. The ferroelectric instability is not restricted to Γ. The branches remain unstable in the Γ–Z–R–X and Γ–X–M planes, however, stiffen rapidly when moving away from the two planes to the A point. These features indicate a 'chain-like' unstable localized distortion for the Nb displacements in real space, similar to what was observed in KN.[33] In addition to the ferroelectric instabilities, at X and M points, rotational instabilities caused by oxygen octahedral tilts around one of the axis can also be clearly observed. For KNNT as shown in Fig. 4, the phonon dispersion also shows the instability of the structure. The modes characterized by the Nb displacement against the octahedron are still unstable along the ΓZ direction. Like those of KNNC, the Na displacement plays an important role in the unstable modes. However, along ZR and ΓX these modes stiffen up away from Z and Γ points and they are stable along RX. Besides the polar unstable modes, along AM, there are still unstable branches corresponding to the oxygen octahedra rotating around the z axis. However, the unstable octahedral rotation modes at X in KNNC become stable in KNNT. For KNNO, only one unstable mode can be observed at R. This mode is dominated by the oxygen octahedra vibrating with significant Na contribution. Except for this mode, all the other phonons are stable. Therefore, the structure of KNNO is more stable than KNNC and KNNT. While for KNNR, no unstable mode can be found from the phonon dispersion, showing the stability of the structure. This is consistent with the fact that the rhombohedral structure $R3m$ is in the ground state of KNN.[34]

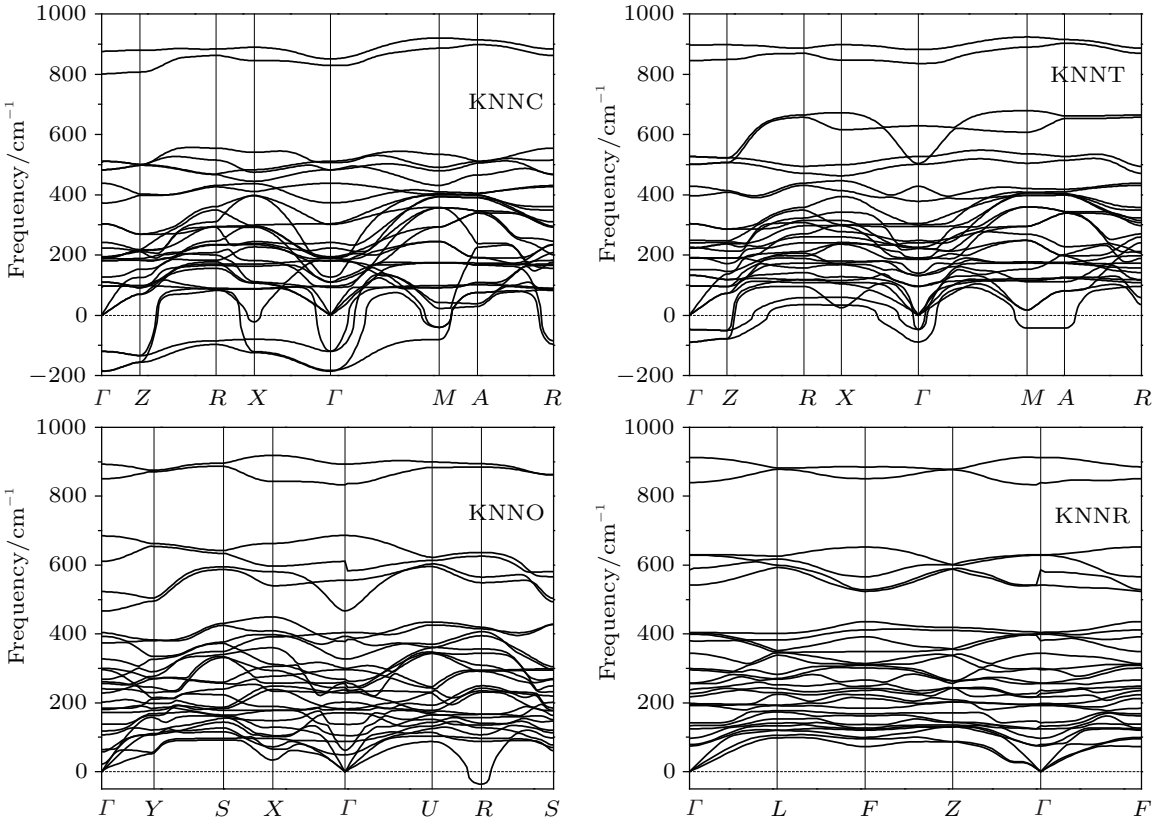


Fig. 4. Phonon dispersions of KNNC, KNNT, KNNO, and KNNR.

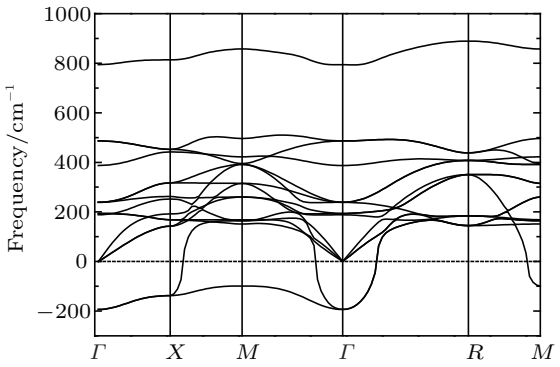


Fig. 5. Phonon dispersions of cubic $KNbO_3$.

For KNNO, the BECs indicate ferroelectric instability along the *x* axis, however, no unstable modes are found along this axis. Zone-center phonon modes are useful properties to gain an insight into the physics of ferroelectric instability. Therefore, we study the zone-center phonon (see Table 4) of KNNO in detail. The zone-center phonons of KNO and NNO are also summarized in Tables 3 and 4, respectively. For NNO, it has an antiferroelectric structure at room temperature. In order to compare with KNO and KNNO, the structure with the space group *Amm*2 is used in our calculations. In the orthorhombic phase *Amm*2 the factor-group analysis yields $4A_1$(IR, R) + $4B_1$(IR, R) +$3B_2$(IR, R)+$1A_2$ (R) optic modes. Hence, 11 modes are simultaneously active in infra-red and Raman spectra, and one is only in Raman-active mode for KNO and NNO. For KNNO, due to the use of a supercell, the space group symmetry reduces to *Pmm*2, therefore the factor-group analysis yields $9A_1$(IR, R) + $9B_1$(IR, R) +$7B_2$(IR, R)+$2A_2$ (R) optic modes. To facilitate the comparison of results among the three compounds, we also calculate the phonon properties of KNO and NNO in *Pmm*2 symmetry which are shown in Table 4. As shown in Tables 3 and 4, for KNO and NNO, minor differences in the calculated phonon frequecy between *Amm*2 and *Pmm*2 symmetries can be found due to the use of truncated basis. However, this has no effect on the analyses of the phonon properties.

The B_2 modes involve only vibrations along the *x* axis; for A_2 modes the in-plane oxygen atoms (O3 and O4) move in opposite directions along the *x* axis with the other atoms staying stationary; for A_1/B_1 modes, K/Na, Nb, and O1 (O2) atoms move along the *b*/*c* axis while O3 (O4) atoms move in the plane perpendicular to the *x* axis. As indicated in Table 3, the calculated frequencies of KNO are in good agreement with the experimental and previous calculated values,[26,35,36] further showing the reliability of our calculated results. For KNO, there is one soft B_2 mode (51.07i) which is a precursor of the orthorhombic-to-rhombohedral phase transition. This mode corresponds predominantly to the Slater mode,[37] with the Nb cations and the oxygen octahedron vibrating oppositely. Therefore, the ferroelectric instability of KNO can be attributed to the displacements of Nb and O atoms along the *x* axis. For NNO, the lowest frequency of B_2 mode, 71.99 cm^{-1}, is assigned to the vibration of Na cation against the oxygen octahedron, commonly known as the last mode[38] and this mode does not show any instabilities of the structure. However, one soft B_1 mode (116.65i) is observed as shown in Table 4. The soft mode is dominated by the in-plane vibration of the in-plane oxygen atom. While for KNNO, the lowest B_2 mode (27.45 cm^{-1}) has contributions not only from the opposite vibrations of the Slater mode but also from Na displacements. Therefore, the driving force of the ferroelectric instability of KNNO can also be attributed to the opposite vibrations of the Nb cations and the oxygen octahedron. However, it can be concluded that the vibrations of Na cations probably have contributions to the ferroelectric phase stability of KNNO compared with the lowest B_2 mode of NNO.

Table 3. Calculated Γ optical phonon frequencies (in cm^{-1}) in comparison with experimental values for KNO and NNO. Imaginary frequencies refer to soft modes.

			KNO				NNO		
Modes	This work		Exp.[35]		Exp.[36]		Cal.[26]	This work	
	TO	LO	TO	LO	TO	LO	TO	TO	LO
B_2	51.07i	186.58	56.00	189.00	40.00		82*i*	71.99	129.50
	192.12	388.56	195.00	425.00	195.00		185	149.39	368.38
	496.26	801.15	511.00	838.00	513.00		467	554.32	866.70
B_1	187.98	188.26	187.00	190.00	192.00		146	81.92	127.14
	233.14	243.60	243.00	264.00	249.00		232	163.26	163.26
	247.21	383.00	270.00	413.00	270.00		297	244.56	360.17
	530.19	821.08	534.00	842.00	534.00		528	589.11	879.21
A_1	191.35	191.66	190.00	193.00	193.00	194.50	186	148.20	162.02
	262.94	275.88	290.00	296.00	281.50	295.00	257	246.71	249.07
	275.88	403.43	299.00	417.00	297.00	434.50	307	278.77	402.13
	581.88	815.30	607.00	827.00	606.50	834.00	593	652.05	875.69
A_2	258.38		283.00		282.00		224	197.58	196.93

Table 4. Calculated Γ optical phonon frequencies (cm^{-1}) for KNNO, KNO, and NNO in *Pmm*2. Imaginary frequencies refer to soft modes.

Modes	KNNO		KNO		NNO	
	TO	LO	TO	LO	TO	LO
B_2	27.45	63.02	60.43i	186.56	69.36	129.53
	65.57	105.41	39.16		74.49	
	118.96	182.74	165.53		112.62	
	185.09	300.14	192.11	388.00	148.49	368.02
	300.14	378.11	312.66		284.95	
	467.42	467.77	423.87		514.84	
	523.52	833.51	496.20	801.14	554.25	866.69
B_1	48.53	56.92	133.75		116.65i	
	87.56	107.06	168.20		82.09	127.26
	170.27	171.50	188.01	188.30	89.00	
	201.34	202.00	233.49	244.03	164.30	164.32
	236.43	240.28	241.66		203.31	
	245.47	326.85	248.21	383.40	245.64	360.92
	326.97	373.37	325.39		328.66	
	557.02	686.24	530.40	821.99	589.18	879.87
	687.67	851.12	661.24		719.89	
A_2	228.78		257.52		196.93	
	296.20		313.71		276.52	
A_1	137.89	142.73	160.81		142.70	
	180.60	182.22	191.34	191.67	148.36	162.02
	257.03	257.69	264.00	276.49	247.57	249.69
	261.08	263.34	264.28		258.99	
	268.67	390.82	276.51	403.55	278.81	402.44
	393.05	400.77	385.84		388.57	
	403.64	405.56	413.76		406.27	
	612.27	843.12	582.05	815.99	651.96	876.11
	893.83	895.41	871.42		916.77	

4. Conclusions

In this work, the electronic structure, BEC, and phonon properties of KNNC, KNNT, KNNO, and KNNR are investigated by the first principles method. The results of the electronic structure indicate a strong covalent interaction between Nb and O atoms which should be responsible for the displacement of Nb and O atoms. The evolutions of BECs and phonon dispersions in the four structures show that the ferroelectric instability of KNN is dominated by Nb and O displacements with significant contributions from Na. Moreover, oxygen octahedron rotation around one axis plays an important role in the rotation instability. In addition, the Γ phonon analysis reveals that Na atoms probably have contributions to the ferroelectric phase stability of KNNO.

References

[1] Egerton L and Dillion D M 1959 *J. Am. Ceram. Soc.* **42** 438
[2] Saito Y, Takao H, Tani T, Nonoyama T, Takatori K, Homma T, Nagaya T and Nakamura M 2004 *Nature* **432** 84
[3] Cakare-Samardzija L, Malic B and Kosec M 2008 *Ferroelectrics* **370** 113
[4] Du J, Wang J F, Zang G Z, Qi P, Zhang S J and Thomas R S 2008 *Chin. Phys. Lett.* **25** 1446
[5] Herber R P, Schneider G A, Wagner S and Hoffmann M J 2007 *Appl. Phys. Lett.* **90** 252905
[6] Hollenstein E, Davis M, Damjanovic D and Setter N 2005 *Appl. Phys. Lett.* **87** 182905
[7] Inagaki Y, Kakimoto K and Kagomiya I 2010 *J. Eur. Ceram. Soc.* **30** 301
[8] Wu J, Xiao D and Wang Y 2008 *J. Am. Ceram. Soc.* **91** 3402
[9] Lin D, Kwok K W and Chan H L W 2008 *J. Phys. D: Appl. Phys.* **41** 045401
[10] Zuo R, Ye C and Fang X 2008 *J. Phys. Chem. Solids* **69** 230
[11] Zhou Y, Guo M, Zhang C and Zhang M 2009 *Ceram. Int.* **35** 3253
[12] Song X P, Zhang Y G, Luo X J, Xu L F, Cao W Q and Yang C P 2009 *Acta Phys. Sin.* **58** 4980 (in Chinese)
[13] Lin D, Li Z, Zhang S, Xu Z and Yao X 2009 *Solid State Commun.* **149** 1646
[14] Kizaki Y, Noguchi Y and Miyayama M 2006 *Appl. Phys. Lett.* **89** 142910
[15] Chen C, Jiang X P, Wei W, Li X H, Wei H B and Song F S 2011 *Acta Phys. Sin.* **60** 107704 (in Chinese)
[16] Hewat A W 1973 *J. Phys. C: Solid State Phys.* **6** 2559
[17] Burton B P and Nishimatsu T 2007 *Appl. Phys. Lett.* **91** 092907
[18] Trodahl H J, Klein N, Damjanovic D, Setter N, Ludbrook B, Rytz D and Kuball M 2008 *Appl. Phys. Lett.* **93** 262901
[19] Ahtee M and Glazer A M 1974 *Ferroelectrics* **7** 93
[20] Ahtee M and Hewat A W 1978 *Acta Cryst.* **A34** 309
[21] Cohen R E and Krakauer H 1990 *Phys. Rev. B* **42** 6416
[22] Cohen R E 1992 *Nature* **358** 136
[23] Niranjan M K, Karthik T, Asthana S, Pan J and Waghmare U V 2013 *J. Appl. Phys.* **113** 194106
[24] Zhong W, King-Smith R D and Vanderbilt D 1994 *Phys. Rev. Lett.* **72** 3618

[25] Ni L H, Liu Y, Ren Z H, Song C L and Han G R 2011 *Chin. Phys. B* **20** 106102
[26] Postnikov A V and Borstel G 1994 *Phys. Rev. B* **50** 16403
[27] Zhang G T, Bai T T, Zhao Y R and Lu C 2013 *Chin. Phys. B* **22** 116104
[28] Milman V, Winkler B, White J A, Pickard C J, Payne M C, Akhmatskaya E V and Nobes R H 2000 *Int. J. Quantum Chem.* **77** 895
[29] Clark S J, Segall M D, Pickard C J, Hasnip P J, Probert M I, Refson K and Payne M C 2005 *Zeitschrift für Kristallographie* **220** 567
[30] Hamann D R, Schlüter M and Chiang C 1979 *Phys. Rev. Lett.* **43** 1494
[31] Gonze X, Beuken J M, Caracas R, Detraux F, Fuchs M, Rignanese G M, Sindic L, Verstraete M, Zerah G, Jollet F, Torrent M, Roy A, Mikami M, Ghosez P, Raty J Y and Allan D C 2002 *Comput. Mater. Sci.* **25** 478
[32] Iniguez J, Vanderbilt D and Bellaiche L 2003 *Phys. Rev. B* **67** 224107
[33] Yu R and Krakauer H 1995 *Phys. Rev. Lett.* **74** 4067
[34] Baker D W, Thomas P A, Zhang N and Glazer A M 2009 *Appl. Phys. Lett.* **95** 091903
[35] Bozinis D G and Hurrell J P 1976 *Phys. Rev. B* **13** 3109
[36] Quittet A M, Bell M I, Krauzman M and Raccah P M 1976 *Phys. Rev. B* **14** 5068
[37] Hlinka J, Petzelt J, Kamba S, Noujni D and Ostapchuk T 2006 *Phase Transitions* **79** 41
[38] Rushchanskii K Z, Spaldin N A and Ležaić M 2012 *Phys. Rev. B* **85** 104109